Desalination 573 (2024) 117210

Contents lists available at ScienceDirect

Desalination

journal homepage: www.elsevier.com/locate/desal

Oil-infused feed spacers for biofouling inhibition

A. Boyko, J.A. Epstein, G.Z. Ramon *

Department of Civil & Environmental Engineering, Technion – Israel Institute of Technology, Haifa 32000, Israel

HIGHLIGHTS

- Oil-impregnated PDMS spacers used to test biofouling prevention
- PDMS stiffness and oil viscosity affect oil uptake and retention.
- Reduced and easily removable biofilm growth on oily substrate
- *E. coli* biofilm mitigation demonstrated on oil-infused PDMS spacer
- Lower viscosity oil and lower stiffness PDMS demonstrate best performance.

ARTICLE INFO

Keywords:
Feed spacer
Biofouling
Oil infused surface
Spiral-wound modules

ABSTRACT

A novel approach is investigated for preventing biofouling of spacer filaments, which are an essential part of spiral-wound modules used in membrane-based desalination. Biofouling, caused by the growth and multiplication of microorganisms on the membrane surface, can significantly impact the efficiency and cost-effectiveness of the desalination process. Herein, a method is proposed for fabricating modified feed spacers based on oil-infused slippery substrates made of polydimethylsiloxane (PDMS). These feed spacers, when infused with silicone oil, create a stable, extremely slippery interface that exhibits exceptionally low bacterial adhesion and prevents biofilm formation, especially under flow conditions. By examining the effect of the silicone oil's viscosity, we determined the optimal ratio of the curing agent for fabricating the oil-infused feed spacer. Results showed a substantial reduction of bacterial adhesion to the surface for all tested oil viscosities, particularly under dynamic conditions. Furthermore, even where bacterial adhesion occurred, primarily on samples infused with lower-viscosity oil, it could be easily removed by simple rinsing. Overall, the oil-infused feed spacer demonstrated exceptional biofilm inhibition, providing preliminary indication of the potential offered by this promising approach.

1. Introduction

Feed spacers are an essential part of spiral-wound NF and RO modules, keeping membranes apart to form the flow channel, as well as promoting mixing. Several studies have established that initial biofouling was formed on feed spacers, and with time these encroached upon the membrane itself [1,2]. As biomass accumulates on the spacer surface, this results in greater resistance to the feed flow and consequently higher feed channel pressure drop, reduced permeate flux and overall lower performance. Some studies have even shown that spacer biofouling is more important than membrane biofouling [3,4].

Enhancing the antifouling properties of spacers can be achieved through two primary approaches. The first approach involves modifying the geometric configuration of the spacer [5], resulting in changes to the hydrodynamic properties of the membrane module. This has been achieved through three-dimensional printing and has shown promise in enhancing membrane module performance. Column and honeycomb-like spacers have demonstrated significant reductions in fouling and biomass accumulation [6,7]. More complex geometries like triply periodic minimal surfaces (TPMS), turbo-spacers, vibrating and helical-type spacers show potential in RO and UF processes [8–11]. Currently, integrating 3D-printed feed spacers into SWM modules faces some challenges, e.g., due to limited flexibility, especially in specialized configurations [12], long-term chemical stability [13], as well as cost [14]. The second approach focuses on directly modifying the surface chemistry of the feed spacer, such as by coating it with biocidal or

* Corresponding author.
E-mail address: ramong@technion.ac.il (G.Z. Ramon).

https://doi.org/10.1016/j.desal.2023.117210
Received 29 May 2023; Received in revised form 13 November 2023; Accepted 2 December 2023
Available online 6 December 2023

biostatic metallic particles (silver and copper) [15], forming nanostructured zinc oxide [16,17] and ZnO nanorods [17], creating silver nanoparticles [18,19], binding chelating ligands charged with metal ions [20], or applying antifouling biomolecules such as polydopamine-g-PEG [21], as well as candle soot nanoparticles (CSNPs) embedded into the ultrathin layer of PDMS coating [22]. These various methods aim to improve the antifouling properties of spacers by directly altering their surface chemistry.

Recently, there has been growing interest in using carbon nanomaterials as coatings, including carbon nanotubes (CNTs) and polypropylene (PP), to produce spacers with improved antifouling properties compared to plain polypropylene spacers [23]. Spacers coated with Laser-Induced Graphene (LIG) have been shown to inhibit biofilm formation and display antiviral and antibacterial effects when an electric current is passed through the material [24]. However, hydrophilic-biocidal (graphene oxide) coatings did not show obvious antibacterial effect [25]. Despite the availability of proposals for low-fouling polymer coatings, including hydrogels and diglyme monomer polymerized in plasma [26,27], none have yet been utilized in the production process.

Herein, we take on a different approach and examine the potential of an oil-infused feed spacer, which supports a thin oil film that represents a low-adhesion interface. The spacer material absorbs a compatible non-polar liquid, immiscible with the outside aqueous environment (the feed channel in the intended application of a membrane module). The impregnated spacer is consequently coated by a thin oil film (the exact properties of which, e.g., its thickness, have yet to be assessed [33,35,38,45]). Similar, Liquid-infused surfaces have recently come to the forefront as a unique approach to surface coatings that can resist adhesion of a wide range of contaminants on medical devices (see, for example, [28,29]). Various studies have shown findings that indicate that there is a variety of liquid infused substrates that have been found to reduce bacterial adhesion to surfaces. Preliminary results of combining perfluorinated or silicone fluids in expanded polytetrafluoroethylene (ePTTE) [30,31], layer by layer (LbL) [32,33] surfaces have been shown to be effective in lowering biofilm formation on the surface of several bacterial strains. In addition, there are preliminary studies in the field of medical applications that have shown the ability of Polydimethylsiloxane (PDMS), infused with silicone oil, to prevent the adhesion of a variety of bacteria to the surface [34,35]. As a proof-of-concept, PDMS is used as a substrate spacer material, which, when combined with silicone oil, creates a liquid-infused surface exhibiting multifunctional properties such as strong mechanical robustness, defect-free self-healing and, most importantly, a liquid-liquid interface leading to a significant reduction of biofouling on the modified spacers, as demonstrated herein.

2. Methods

2.1. Fabrication of fluorescently labeled, oil-infused substrates

Samples were fabricated using PDMS (Dow Sylgard 184 polydimethylsiloxane). The polymeric base was mixed with the curing agent at 5:1 and 10:1 ratios, to produce PDMS with different stiffness and oil infusion capacity. The infused silicone (iPDMS) samples are then prepared by immersing the cured PDMS in silicone oil with viscosities of 10, 20, 100 or 1000 cSt (Sigma-Aldrich). In order to facilitate visualization, the silicone oil was mixed with a fluorophore (Dye-Lite, Tracer products) with an *excitation/emission* peak at 515/600 nm.

2.2. Bacterial cultivation

As a model biofilm-forming bacteria, a pure green fluorescent protein (GFP) *E. coli* culture was used, at a concentration of 10^7 CFU/mL (OD of 0.7). The bacterial culture was grown in Luria Broth (LB) containing kanamycin (Sigma-Aldrich) at a concentration of 0.5 μl/ml for 24 h at 37 °C in an orbital shaker under 105 rpm.

2.3. Planar surface bio-growth under static and dynamic conditions

Biofilm formation on iPDMS samples was tested under static and dynamic tilting (performed at 125 RPM in an orbital shaker), as schematically shown in Fig. 1a. Substrate samples were placed in 50 mL test tubes filled with bacterial suspension. For each experiment, two control samples and two infused samples were tested. The test tubes are placed into an incubator for 24 h at 30 °C. After each experiment, samples were dipped into saline solution (gentle rinse) to wash off non-attached, planktonic bacteria. Samples were then imaged under the microscope.

2.4. Silicone oil removal by flow

PDMS samples were subjected to fluid shear in order to test the dynamics of the infused silicon oil release, over a 5-day period. The PDMS samples are weighed prior to each experiment. Each sample is then infused with silicon oil of varying viscosities: 10, 20, 100 and 1000 cSt. The dynamic tilting experiment is performed using deionized water (as explained in Section 2.3). The samples are then weighed every 24 h, in order to measure the loss of the impregnated oil. Following 5 days of oil release, the samples are subjected to the dynamic tilting experiment for 24 h with a bacterial suspension and are subsequently imaged using a confocal microscope (SP8, Leica).

2.5. Fabrication of iPDMS feed spacer

The iPDMS feed spacers were fabricated using an aluminum mold shaped with the feed spacer geometry. In the fabrication, liquid PDMS was poured onto the mold, followed the procedure previously explained to form PDMS (see Sub-section 2.1) using only 10:1 ratio. The radius of the spacer filament is 0.5 mm while the radius of the cross section is 0.8 mm. The tested feed spacers (iPDMS spacer) were infused with 20 and 100 cSt silicone oil.

2.6. PDMS feed spacer flow experimental system

The experimental system consists of 4 transparent and disposable flow cells, in which infused feed spacers are placed. The feed, bacteria suspended in LB, is continuously pumped into the cells using a high precision syringe pump (PHD ULTRA, Harvard Apparatus) with a four-syringe head - one for each cell. The system is operated without recirculation of the feed and negligible pressure inside the flow cells and tubes (see Fig. 1b). In all experiments, two out of the four flow cells contain control samples (spacers without oil), while the other two cells contain oil-infused feed spacers. The experiments are run for 24 h under a constant flow rate of 41.4 μL/min, which corresponds with a shear rate of 2 [s^{-1}]. At the end of each experiment, all the flow-cells were rinsed with a 10 mL sterile saline syringe.

2.7. Imaging biofilm growth via confocal microscopy

For imaging of the spacers and the biofilm formed, a confocal microscope (Leica TCS SP8, Leica Microsystems, Germany) is used, with either a water-immersion, 25× objective or an air 10× objective. Each sample is imaged in at least 3 different areas. In the feed spacers, two regions were imaged: the filament and the cross section (see Fig. 2). Since the spacer itself is not fluorescent, bright field imaging is used, onto which the fluorescently-detected biofilm is superimposed. The excitation/emission of the GFP *E. coli* is 490/520 nm, while the excitation-emission of the Dye-Lite, used in the oil, is 560/630 nm, which enabled clear differentiation.

2.8. Image processing

To quantify the biofilm growth from images obtained by the confocal microscope, two MATLAB-based algorithms were employed - one for

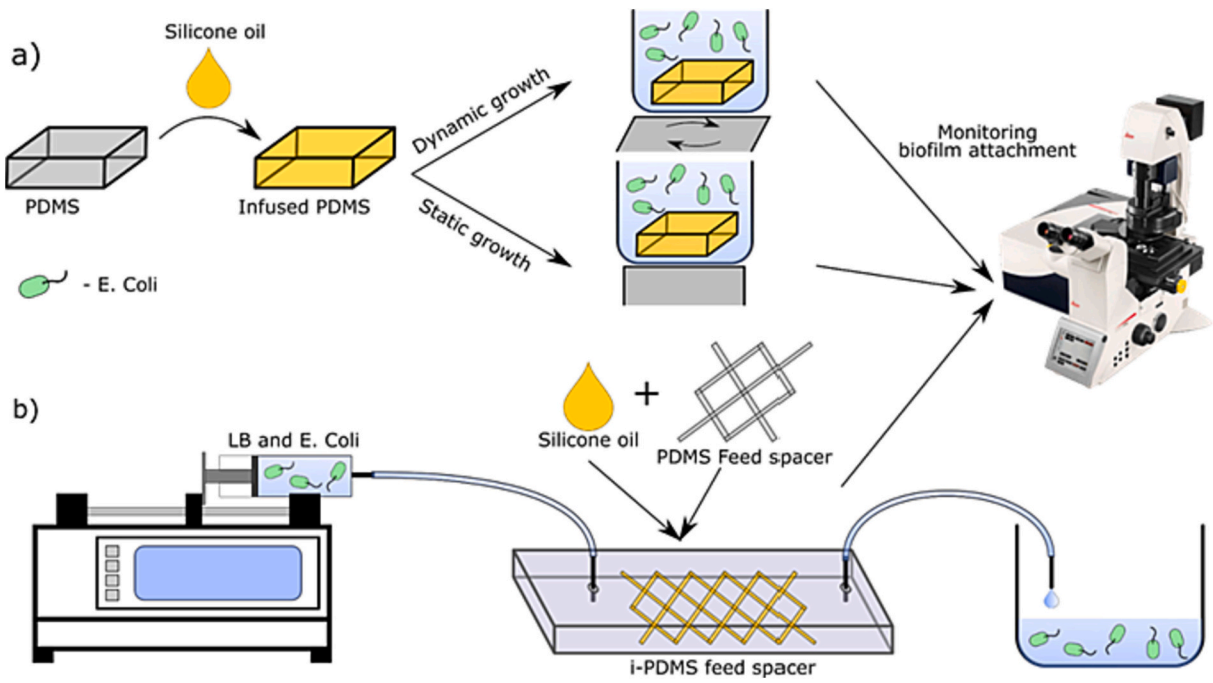

Fig. 1. Schematic of the experimental procedure. a) System for static and dynamic biofouling assay (Section 2.3) iPDMS sample undergoing either dynamic or static growth. b) Feed spacer flow experimental system (Section 2.6). Bacterial suspension is continuously pumped into the cell containing the feed spacer. In both cases, biogrowth experiments are followed by microscopic imaging.

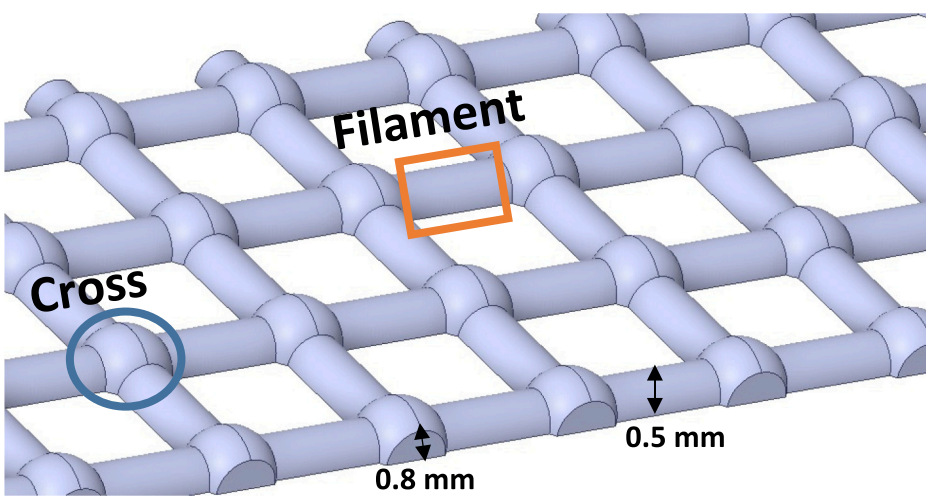

Fig. 2. Illustration of the fabricated feed spacer geometry, measurements, and defined regions for biogrowth quantification.

analyzing the area coverage of the biofilm, and another to quantify the volume of the biofilms. The fluorescence images are first converted to 8-bit gray-scale images, corresponding with values of light intensities between 0 and 255. A light-intensity threshold is then applied to the images, to distinguish between the pixels where the biofilm is present, and noise or out-of-focus signal. The biofilm area coverage is calculated by counting the pixels that contain a light-intensity value above the fixed threshold. Since all experiments are performed using the same imaging properties (laser power, objective, pinhole, gain from the light detector, and pixel size), we compare the area coverage datasets by displaying the data as normalized area coverage, employing the following formula:

$$\mathrm{Xnorm} = (\mathrm{X} - \mathrm{Xmin})/(\mathrm{Xmax} - \mathrm{Xmin})$$

where X_{norm} is calculated individually for the defined dataset. The maximum value of the parameter X in that dataset is represented as X_{max}, while similarly X_{min} represents the minimum value for that dataset. Therefore, in a figure showing normalized area coverage, the value of '1' corresponds to the X_{max} value evaluated from the dataset shown in that figure.

For the biofilm volume, three-dimensional images are reconstructed using the confocal microscope. Biovolume (μm^3) is defined as the number of pixels in which the biofilm is present, multiplied by the voxel size. The datasets are represented as bar charts, where each category displays the mean value and the error bars represent the standard error (SE), calculated as: $SE = \frac{SD}{\sqrt{n}}$, where SD is the standard deviation and n represents the sample size.

3. Results and discussion

3.1. Characterization of silicone oil infused PDMS

The successful establishment of an oil-infused substrate supporting a liquid film necessitates precise adjustments of surface and interfacial energies tailored to the specific application [31,36]. An exemplary illustration of such materials is the oil-infused polydimethylsiloxane elastomer, a derivative rooted in silicone. iPDMS encompasses unbound polymer chains of silicone oil within a cross-linked silicone elastomer, forming a swollen polymer network [37].

Silicone exhibits exceptional receptiveness to solvent infusion due to the notably low rotational energy barrier around the Me_2Si—O bond (3.3 kJ/mol). This characteristic facilitates seamless diffusion throughout the polymer matrix. Consequently, this infusion confers slippery attributes to PDMS, resulting from the establishment of a liquid layer on its surface. The presence and stability of this layer are contingent upon achieving a delicate equilibrium between fluid shear and the interaction between the oil and polymer substrate [38]. In essence, this process involves the absorption and expansion of a polymer in an environment where the solvent is chemically compatible and the degree of swelling diminishes with the rigidity of the polymer network. While PDMS and silicone oil are used here as part of the proof-of-concept, other materials with possibly similar synergy can be tested in future work, once the concept has been further verified.

The ratio of PDMS base to curing agent, and the viscosity of the infused silicone oil can be used to adjust the matrix properties of the PDMS which, in turn, can be used to optimize the fabrication of an anti-fouling feed spacer system. To quantify and interpret how such changes affect the oil-infused PDMS, samples with different base-to-curing agent ratios (5:1 and 10:1 by weight) were submerged in silicone oils with viscosities of 10, 20, 100, and 1000 cSt as summarized in Table 1. The silicone oil absorption was defined as the ratio W/W_t, where W is the mass of the adsorbed oil and W_t is the mass of polymer with the oil. The PDMS and silicone oil pairing resulted in an infused PDMS with increased mass and volume, reaching equilibrium after immersion for approximately 24 h.

The maximum oil uptake was observed using the lowest viscosity oil (10 cSt) at a 10:1 ratio, resulting in an uptake of 42.5 %, and slightly less for a 5:1 ratio, resulting in an uptake of 39.6 %. This trend was observed in the case of PDMS made at a 10:1 ratio of base to curing agent with 20 cSt oil, with an uptake of 36.4 % for a 10:1 ratio and 34.1 % for a 5:1 ratio. However, the PDMS ratio did not have any significant impact on oil adsorption at a viscosity of 100 cSt. The overall oil uptake for both ratios was primarily influenced by an increase in viscosity. Notably, a similar tendency was observed for the highest viscosity oil (1000 cSt), with the lowest amount of oil absorption occurring for both ratios of the PDMS.

The data suggest that, as is expected for any polymer network, the degree of swelling in oil-infused PDMS predominantly depends on the base to curing agent ratio, which represents the rigidity of the polymer network, while the oil viscosity has a far less pronounced effect. This is consistent with observations made for PDMS swelling in chloroform, which showed that the degree of swelling increased with increasing base-to-curing agent ratio [39]. Moreover, the various percent change in mass based on the viscosity and the PDMS ratio may indicate differences in the equilibrium constants of the system [40]. These findings may be explained by the average molecular weight of the polymer chains between the crosslinks [41].

Table 1
Silicone oil removal percentage during orbital shaking - dynamic flow condition.

PDMS ratio	Oil viscosity (cSt)	Overall released oil %	$\%\frac{W}{W_t}$
10:1	10	3 ± 0.6	42.5 ± 1.4
	20	2.2 ± 0.5	36.4 ± 0.7
	100	14.7 ± 5.4	20.9 ± 2.5
	1000	48.1 ± 2	7.9 ± 1.3
5:1	10	4.8 ± 0.5	39.6 ± 1
	20	3.4 ± 0.1	34.1 ± 0.8
	100	16.5 ± 3.2	20.7 ± 1.4
	1000	60.9 ± 4.8	14.8 ± 3.4

The dimensions and oil content of infused PDMS can be adjusted by altering of both the curing agent ratio and oil viscosity. A higher equilibrium volume fraction of oil can be achieved by decreasing the oil viscosity and/or increasing the curing agent mixing ratio. In practical applications, the durability of the lubricated system is evaluated by subjecting the oil overlayer to external forces or interfaces that strip away the liquid. Fig. 3 shows the results of iPDMS samples that were subjected to continuous orbital shaking (120 rpm) for 5 days. The percentage of oil loss was calculated for each day and overall. It was found that the lower the viscosity of the oil, the lower the release percentage of the oil, regardless of the ratio. The most successful combination was a 10:1 ratio of PDMS with a 20 cSt oil, which loses 2.2 % of the oil, compared to a 5:1 ratio with the same oil, which loses 3.4 %. The results also indicated that an increase in the curing ratio resulted in a better ability of the PDMS to retain the silicone oil, leading to lower oil release. Additionally, it was observed that the release of the oil from the PDMS reaches apparent equilibrium (i.e., at the time scales being considered, the changes in oil content falls below the measurement threshold) after ~72 h of vigorous shaking conditions, in all cases tested. This result demonstrates very good retention of the coating where measured oil release became insignificant over time, and the ability of iPDMS to maintain a stable oil overlayer under flow conditions for an extended period.

3.2. Biofilm growth on pre-conditioned iPDMS under applied shear

Next, we examine biogrowth on pre-conditioned samples, that is, samples impregnated with oil and then shaken for 5 days, thus removing excess oil up to the point where measured oil release became insignificant over time. Following the biogrowth under orbital shaking, confocal images were taken after dipping the samples in saline solution to remove any planktonic bacteria. As seen from Fig. 4a, there is an apparent visual difference between the control, untreated PDMS (1), and mainly the 100 and 10 cSt infused PDMS (3 + 4) for both 10:1 and 5:1 curing ratios. However, for the sample infused with the 1000 cSt oil (2), a more prominent biofilm was formed, similar to the untreated control sample. Finally, Fig. 4a (4) presents a sample infused with 10 cSt oil, which exhibited minimal biofilm formation under the applied orbital shaking. To better assess the visual results, image analysis was performed, as described in Section 2.8, with results normalized to the highest biofilm area coverage value of the non-infused PDMS control sample.

The results of the normalized bacteria area coverage for two PDMS ratios are presented in Fig. 4b. It can be seen that there is a decrease in the biofilm coverage over the samples in both ratios, which is affected by the decreasing viscosity of the infused silicone oil. Thus, in samples with an oil viscosity of 10 and 20 cSt almost no biofilm is seen for both curing ratios. It can be inferred that there is a high impact of the initial infused oil percentage at equilibrium with the ability to preserve the oil in the substrate (due to the high affinity of the oil to the polymer chains of the PDMS) during the exposure to shear, on the capability to inhibit biofilm formation. Furthermore, iPDMS demonstrates the concept of keeping surface slippery performance via self-replenishment from within the PDMS, which serves as a reservoir for oil. Hence, in the event of depletion of the oil layer due to complete oil leaching, a liquid oil layer will cease to be present on the surface, impeding its ability to deter bacterial adhesion. This is evident in some of the conditions tested - for both curing ratios, 10:1 and 5:1, infused with 1000 cSt oil, a relatively small amount of oil was infused, corresponding with an oil loss of about 48.1 and 60.9 %, consequently eliminating the non-fouling properties of iPDMS as bacteria may adhere more strongly to the areas where the

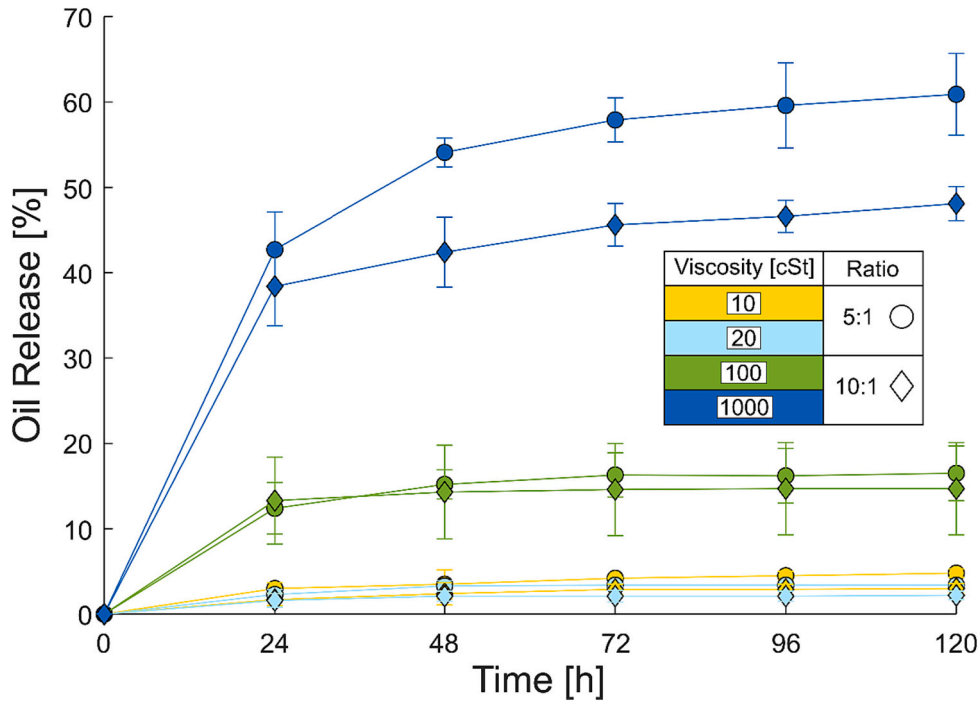

Fig. 3. The dynamics of Silicone oil release, for different oil viscosities, shown as the percent change in the mass of oil in the sample, released from the infused PDMS under orbital shaking (dynamic conditions), using 5:1 and 10:1 ratio PDMS.

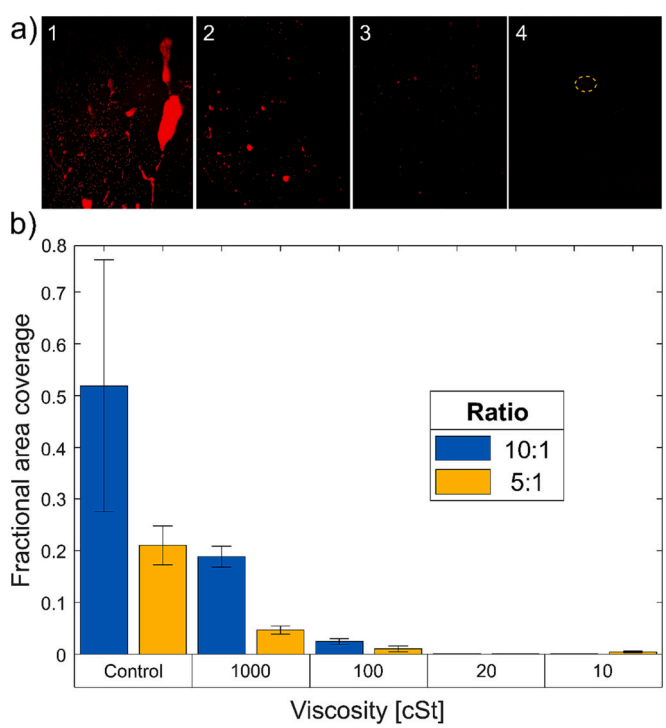

Fig. 4. a) Representative confocal images of biofilm formation under dynamic flow following five days oil release. Images labeled 1, 2, 3, 4 represent control, 1000, 100 and 10 cSt, respectively. b) Fraction of sample area covered by a biofilm formed under dynamic orbital shaking following five days of oil release. Samples used were either a 5:1 or 10:1 iPDMS with 1000, 100, 20, 10 cSt oil.

infused liquid layer is depleted. On the other hand, for lower viscosity samples, a higher amount of oil was absorbed and less oil was released as the viscosity was reduced. This provides continuous slippery properties to the anti-fouling iPDMS. Our five-day experiment substantiates that the substrate effectively maintains the oil layer without any discernible leakage. As observed in a separate study, such materials can maintain anti-fouling capabilities for up to several months [42]. Fig. 4b shows that the biofilm coverage is lower for most viscosities in a 5:1 sample, compared to the sample with a 10:1 curing ratio. Meanwhile, at low viscosities - 10 cSt and 20 cSt - the difference is negligible. Another recent study showed that *E. coli* attachment onto PDMS samples appeared to be stronger on softer surfaces than harder surfaces [43]. Additionally, another study showed the lowest contact angle hysteresis (CAH, which is a direct indicator of nonstick properties of a solid surface [44]) for a 5:1 ratio compared to 10:1 and 20:1 ratios, and suggested that decreased PDMS stiffness could be playing an increasing role in the greater contact angle hysteresis; therefore, the stability of a low CAH is essential for resisting bacterial adhesion [45]. Silicone oil with higher viscosity exhibits increased surface tension: 1000 cSt has a surface energy of 35 mN/m, while 100 cSt has 20.9 mN/m. This low surface tension, along with its surface-occupying capability, leads to a water-repellent coating that may reduce bacterial adhesion. iPDMS surfaces demonstrate lower Contact Angle Hysteresis (CAH) compared to PDMS, indicating non-adhesive properties. iPDMS also displays a smooth surface with a low sliding angle (2.1 ± 0.9°), while PDMS shows higher angles (40.1 ± 9.0°) [38].

3.3. Biofilm growth on iPDMS under static and dynamic conditions

The present study aimed to investigate the effectiveness of an oil-infused substrate in preventing biofilm growth under static conditions, where there is no flow or shear, and to compare it to dynamic conditions, under the effect of shear forces due to flow in the spacer channel, and quantify the impact on bacterial attachment and biofilm growth. To do this, samples were made with different curing agent ratios (10:1 and 5:1) and silicone oil viscosities (10, 100, and 1000 cSt).

As seen in Fig. 5a, there is a significant visual difference between the untreated control PDMS samples (A1, B1) and the infused PDMS samples (A2/3, B2/3) under both static and dynamic conditions. The iPDMS surface demonstrated overall less bacterial attachment, where as expected, more bacteria were present under static conditions than under

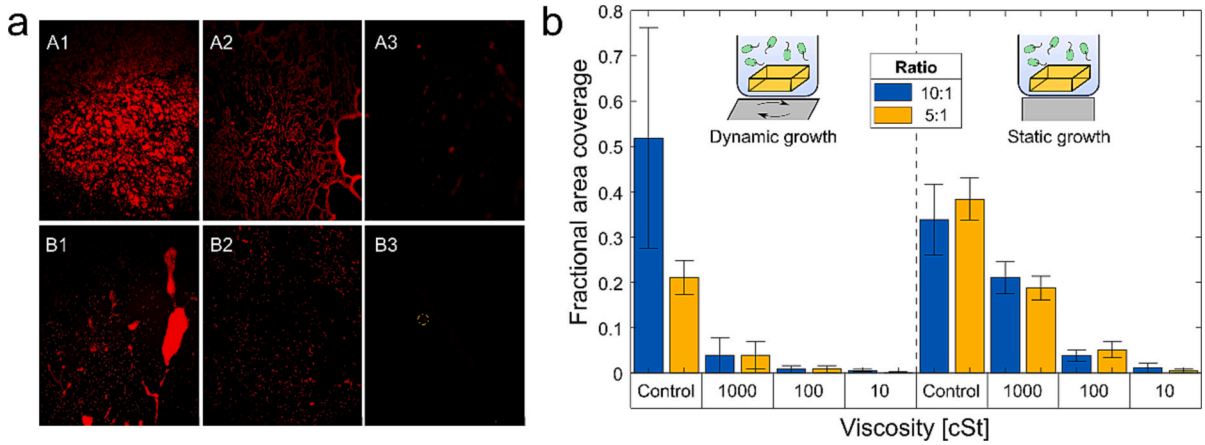

Fig. 5. Biofilm formation on PDMS after a 24 h period under dynamic and static flow conditions. a) Representative confocal images of florescence biofilm formation under static and dynamic flow (A, B) respectively. (1, 2, 3) Control, 1000 cSt, 10 cSt respectively. b) Biofilm normalized area coverage using image analysis.

dynamic conditions. Additionally, a decrease in oil viscosity corresponded with a decline in biofilm area coverage.

To better assess these visualization results, image analysis was conducted to calculate the area coverage (normalized with respect to the highest area coverage, which for this case is the PDMS control), as seen in Fig. 5b, enabling a more quantitative comparison. The image analysis confirmed that significantly more biofilm adhesion occurred under static than dynamic conditions. For instance, samples infused with 1000 and 100 cSt silicone oil and exposed to dynamic conditions had approximately 5 times less biofilm area coverage. Similarly, samples infused with 10 cSt silicone oil under dynamic flow had approximately 3 times less biofilm area coverage than those under static conditions. The minimal (practically no biofilm) adhesion observed in the samples under dynamic conditions can be attributed to the shear force produced by the flow, which likely removes bacteria and their extracellular polymeric substances (EPS) or otherwise interferes with the adhesion.

Results also demonstrate that the viscosity of infused oil significantly impacts the strength of bacterial adhesion, with higher viscosity of the infused oil resulting in stronger adhesion. With an identical rinsing step, following biogrowth, samples impregnated with lower viscosity oil exhibited greater removal of bacteria. This suggests that even when a biofilm does form on the iPDMS surface, it can be easily removed under higher shear conditions due to the weak adhesion of the biofilm to the liquid interface.

3.4. Biofilm formation on iPDMS feed spacers

Based on results presented in the previous sections, it was concluded that iPDMS feed spacers would be fabricated using a base-to-curing agent ratio of 10:1, and infused with 100 cSt and 20 cSt silicone oil. The choice of the 10:1 ratio was based on the observation that it exhibited better oil retention, while preserving the slippery surface functionality. Within a spacer infused with lower viscosity oils of 10 and 20 cSt, a pronounced affinity is observed between PDMS and the oil. A minimal quantity of oil is released into the liquid under the influence of shear forces, as indicated in Fig. 1. Based on these observations, it is posited that the likelihood of oil fouling caused to the membranes is very low. Of course, long-term tests would still be required in order to assess this under real-world conditions. The 100 cSt silicone oil effectively inhibited biofilm formation without significant changes in sample volume, while the 20 (and 10 cSt) silicone oil showed slightly better biofilm inhibition, but at the cost of absorbing more oil and increasing spacer volume, with 10:1 feed spacers exhibiting a filament size increase of ~12 % when infused with 100 cSt oil, ~22 % with 20 cSt oil, and ~27 % with 10 cSt oil. In order to verify the uniform distribution of the infused oil, it was premixed with Dye-Lite, a fluorescent material, and then visualized by confocal microscopy, as seen in Fig. 6. A noteworthy study of oil-infused PDMS utilized a confocal microscope in an attempt to quantify the oil layer thickness [34]. For a 10 cSt oil in a 10:1 PDMS, the reported thickness exhibits varying degrees of uniformity, spanning a range of 15 to 35 μm, likely reflecting some degree of underlying roughness. It is reasonable to infer that the thickness of an oil layer for a viscosity of 20 cSt should closely align with these values [34]. When assessing future integration of new spacers into SWMs, it would be important to evaluate their robustness under all operating conditions, including possible chemical cleaning. While no data exists directly related to iPDMS and its reaction to acids, bases, or hypochlorites, one may draw on evidence related to PDMS and silicone oil. Following recognized RO membrane cleaning protocols [46,47], PDMS shows no adsorption or dissolution when in contact with common cleaning substances [48]. There's a possibility of gradual hydrolytic degradation under extreme pH after continuous exposure for days, but no adverse effects expected after a few hours of cleaning at ambient temperature [49]. Additionally, PDMS demonstrates resilience in the presence of hypochlorites [50]. We also note that, given the functionality of the spacer, the need for clean in place (CIP) practices may be reduced considerably. Of course, in any future implementation at module scale, these aspects will need to be verified.

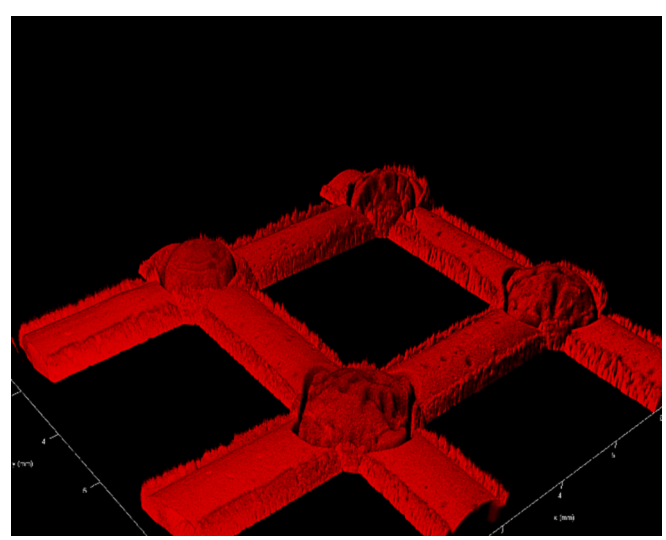

Fig. 6. 3D Confocal image of fluorescent-labeled, 100 cSt silicone oil infused into the PDMS feed spacer.

3.5. iPDMS feed spacer under flow conditions

Biofilm formation experiments were conducted under flow conditions to evaluate the ability of 20 cSt and 100 cSt silicone oil iPDMS feed spacers to inhibit biofilm formation. Fig. 7a shows the results, with an image (A) representing the control PDMS feed spacer, and images (B) and (C) showing the 20 cSt and 100 cSt iPDMS feed spacers, respectively. The results indicate a clear difference between the control and iPDMS spacers. The control spacer was utterly covered with biofilm, which was not washed off and irreversibly attached to the spacer. In contrast, the iPDMS spacer had only a few areas (marked with a red dotted line) where biofilm was present as a thin layer with low brightness, distinctively different from the thick, uniform biofilm coating seen on the control spacer. The biofilm seen on the iPDMS image may have been partially bonded to the cover glass of the cell rather than to the iPDMS feed spacer. Fig. 7b shows the results of the biovolume for the PDMS feed spacer, 20 cSt and 100 cSt iPDMS feed spacers. The 100 cSt iPDMS feed spacer had approximately one order of magnitude less biovolume than the control feed spacer, while the 20 cSt iPDMS feed spacer had approximately two orders of magnitude less biovolume. These results demonstrate that shear forces can significantly decrease the initial formation of biofilms on the surface of iPDMS, while enabling the subsequent removal of biofilms. Even at low shear conditions (which are much lower than those used in membrane systems, as we wanted to evaluate the anti-fouling properties of iPDMS under more favorable biofouling conditions), a significant reduction in biofilm was observed. Since the surface's hydrophobicity remains unchanged after lubricant infusion, this effect can be attributed to the mobile liquid overlayer coating, which acts as a barrier to adhesion preventing bacteria from probing and forming bonds on the solid surface, making it a difficult attachment site for the bacteria.

3.6. Biofouling growth inhibition on key regions of the feed spacer

The spacer generates complicated hydrodynamics due to the obstruction it represents to the flow. The main point of aggravated fouling is normally at the cross-filament sections, where the flow is mostly stagnant; conversely, regions along the center of filaments are exposed to the most direct crossflow impingement, and therefore substantial shear forces that are expected to inhibit biofilm development. Experiments were conducted to investigate the effects of an oil-infused surface on the formation of biofouling on these two regions, performed under the same flow conditions.

As seen in Fig. 8b, the iPDMS spacer filament area is marked in orange, and the cross-section area is marked in blue. In Fig. 8a, Row A and C represent the control PDMS area of cross-section and filament, respectively, while Row B and D represent the iPDMS cross-section and filament area, respectively. As shown in Fig. 8a, there was a significant reduction in biofilm formation on the cross-section and filament area of the iPDMS spacer, as compared to the control spacer areas where substantial biofouling was observed on the surface of the cross-section and filament. In the figure, the observed areal coverages were normalized based on the highest single observation and differentiated by the regions of 'filament' and 'cross section' (as illustrated in Fig. 2). For the two PDMS areas presented in Fig. 8b, it can be observed that there is a drastic decrease in the biofilm coverage over the samples in both areas, which is attributed to the slippery surface of the oil-infused feed spacer. Additionally, previous studies have reported that biofouling initially occurs at the spacer cross junctions [51], which is consistent with the findings of this experiment that more biofilm coverage was observed in the cross-junction area. Therefore, using oils with lower viscosity, such as 20 cSt, may further decrease and inhibit the initial attachment of biofilm to the feed spacer in the cross-junction area, as the oil-infused surface reduces biofilm adhesion.

4. Conclusions

In this work, we characterized the tunability of silicone oil-infused PDMS with varying curing agent concentrations and oil viscosity, in order to produce a biofilm-inhibiting feed spacer. In exploring the effect

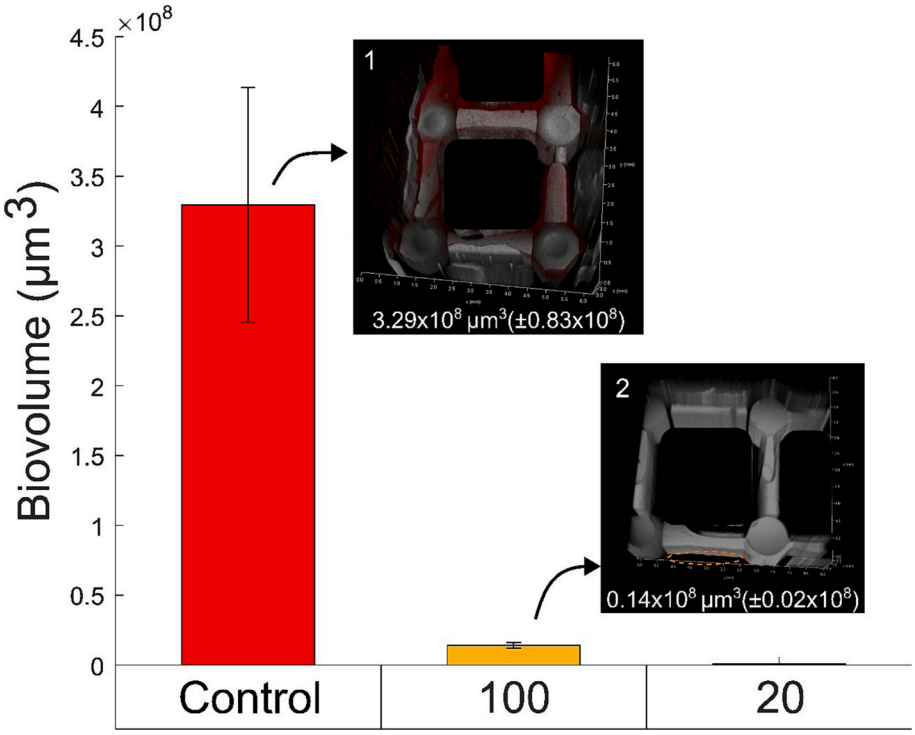

Fig. 7. Biovolume using image analysis on 10:1 ratio untreated control PMDS and iPDMS feed spacers with 100, 20 cSt silicone oil after 24 h flow experiment, representative confocal three-dimensional image: Untreated control PMDS feed spacer (1) and 100 cSt iPDMS feed spacer (2).

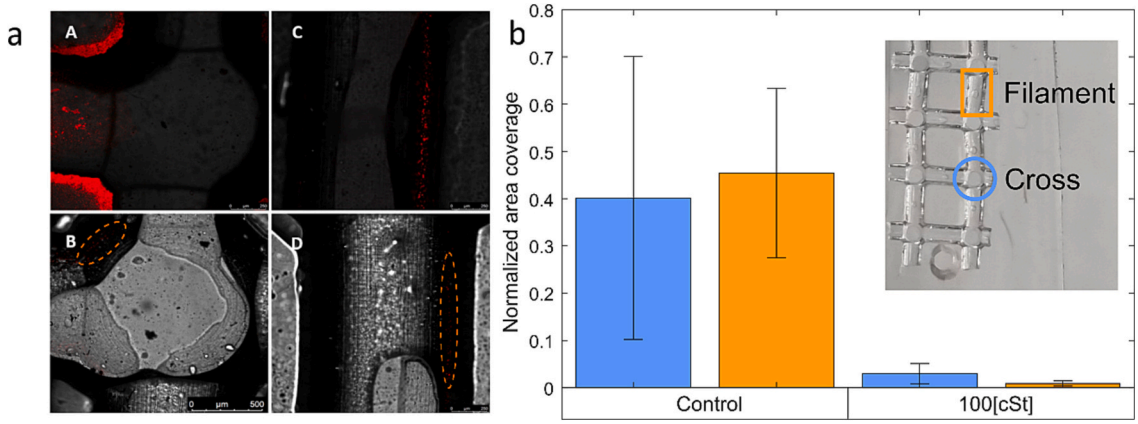

Fig. 8. Biofilm formation on 10:1 PDMS and 100 cSt iPDMS feed spacers in cross, filament sections after 24 h flow condition. a) Representative Confocal images of the scan section. (A, C) Control PDMS Cross, filament area respectively. (B, D) iPDMS cross, filament area. The red circles indicate areas with biofilm. b) Biofilm normalized area coverage using image analysis on PDMS and iPDMS filament and cross areas on feed spacer.

of curing agent concentration and oil viscosity on both the total oil uptake and stability of the immobilized liquid, it was found that with a decrease in oil viscosity and/or increase in curing agent mixing ratio, the sample can absorb more oil and, more importantly, retain the oil when the over-layer is subjected to external fluid shear. In general, a combination of polymer stiffness and oil viscosity determined uptake and stability over time, which also impacted biofilm inhibition.

As the main outcome of this study, it has been demonstrated that *E. coli* biofilm formation can be drastically reduced under flow conditions, within a flow-cell that mimics the general characteristics of a spacer-filled channel within a spiral-wound membrane module. It was first shown, on iPDMS samples, that even where some biogrowth had occurred, a simple saline rinse resulted in complete or near-complete biofilm removal. This was in sharp contrast with the control PDMS surfaces, where adherence was mostly irreversible. Even in the absence of flow and shear, under static conditions, a significant reduction in biofilm development was observed.

Since interfacial properties are assumed to remain essentially unchanged after lubricant infusion, due to the chemical similarity, the decreased biofilm development can be explained by the mobility of the liquid overlayer. The fluid layer prevents bacteria from probing and forming bonds on the solid surface, making it difficult for attachment. While further research is required to understand the exact mechanisms of bacterial attachment and detachment from the oil-infused surface, the presented results clearly demonstrate the potential that iPDMS spacers provide for biofouling prevention in membrane separation.

CRediT authorship contribution statement

A. Boyko: Conceptualization, Methodology, Validation, Formal analysis, Investigation, Writing – original draft, Writing – review & editing, Visualization. **J.A. Epstein:** Software, Formal analysis, Data curation, Writing – review & editing, Visualization. **G.Z. Ramon:** Conceptualization, Methodology, Resources, Validation, Writing – original draft, Writing – review & editing, Visualization, Supervision, Funding acquisition.

Declaration of competing interest

The authors declare the following financial interests/personal relationships which may be considered as potential competing interests: Guy Ramon reports financial support was provided by Israel Science Foundation.

Data availability

No data was used for the research described in the article.

Acknowledgements

The research was supported by the Israel Science Foundation, grant 3041/21.

References

[1] J. Baker, T. Stephenson, S. Dard, P. Côté, Characterisation of fouling of nanofiltration membranes used to treatsurface waters, Environ. Technol. (U. K.) 16 (1995), https://doi.org/10.1080/09593331608616335.

[2] S.S. Bucs, A.I. Radu, V. Lavric, J.S. Vrouwenvelder, C. Picioreanu, Effect of different commercial feed spacers on biofouling of reverse osmosis membrane systems: a numerical study, Desalination 343 (2014), https://doi.org/10.1016/j.desal.2013.11.007.

[3] J.S. Vrouwenvelder, C. Picioreanu, J.C. Kruithof, M.C.M. van Loosdrecht, Biofouling in spiral wound membrane systems: three-dimensional CFD model based evaluation of experimental data, J. Membr. Sci. 346 (2010), https://doi.org/10.1016/j.memsci.2009.09.025.

[4] A.I. Radu, M.S.H. van Steen, J.S. Vrouwenvelder, M.C.M. van Loosdrecht, C. Picioreanu, Spacer geometry and particle deposition in spiral wound membrane feed channels, Water Res. 64 (2014) 160–176, https://doi.org/10.1016/j.watres.2014.06.040.

[5] A. Siddiqui, N. Farhat, S.S. Bucs, R.V. Linares, C. Picioreanu, J.C. Kruithof, M.C. M. Van Loosdrecht, J. Kidwell, J.S. Vrouwenvelder, Development and characterization of 3D-printed feed spacers for spiral wound membrane systems, Water Res. 91 (2016), https://doi.org/10.1016/j.watres.2015.12.052.

[6] S.M. Ali, A. Qamar, S. Kerdi, S. Phuntsho, J.S. Vrouwenvelder, N. Ghaffour, H. K. Shon, Energy efficient 3D printed column type feed spacer for membrane filtration, Water Res. 164 (2019) 114961, https://doi.org/10.1016/J.WATRES.2019.114961.

[7] N. Yanar, M. Son, H. Park, H. Choi, Bio-mimetically inspired 3D-printed honeycombed support (spacer) for the reduction of reverse solute flux and fouling of osmotic energy driven membranes, J. Ind. Eng. Chem. 83 (2020) 343–350, https://doi.org/10.1016/J.JIEC.2019.12.007.

[8] N. Sreedhar, N. Thomas, O. Al-Ketan, R. Rowshan, H. Hernandez, R.K. Abu Al-Rub, H.A. Arafat, 3D printed feed spacers based on triply periodic minimal surfaces for flux enhancement and biofouling mitigation in RO and UF, Desalination 425 (2018), https://doi.org/10.1016/j.desal.2017.10.010.

[9] S.M. Ali, A. Qamar, S. Phuntsho, N. Ghaffour, J.S. Vrouwenvelder, H.K. Shon, Conceptual design of a dynamic turbospacer for efficient low pressure membrane filtration, Desalination 496 (2020), https://doi.org/10.1016/j.desal.2020.114712.

[10] Y.Z. Tan, Z. Mao, Y. Zhang, W.S. Tan, T.H. Chong, B. Wu, J.W. Chew, Enhancing fouling mitigation of submerged flat-sheet membranes by vibrating 3D-spacers, Sep. Purif. Technol. 215 (2019), https://doi.org/10.1016/j.seppur.2018.12.085.

[11] S. Kerdi, A. Qamar, A. Alpatova, J.S. Vrouwenvelder, N. Ghaffour, Membrane filtration performance enhancement and biofouling mitigation using symmetric spacers with helical filaments, Desalination 484 (2020), https://doi.org/10.1016/j.desal.2020.114454.

[12] N. Yanar, M. Son, E. Yang, Y. Kim, H. Park, S.E. Nam, H. Choi, Investigation of the performance behavior of a forward osmosis membrane system using various feed spacer materials fabricated by 3D printing technique, Chemosphere 202 (2018) 708–715, https://doi.org/10.1016/J.CHEMOSPHERE.2018.03.147.

[13] J.W. Koo, J.S. Ho, J. An, Y. Zhang, C.K. Chua, T.H. Chong, A review on spacers and membranes: conventional or hybrid additive manufacturing? Water Res. 188 (2021) 116497, https://doi.org/10.1016/J.WATRES.2020.116497.
[14] J. Johnson, M. Busch, Engineering aspects of reverse osmosis module design, Desalination Water Treat. 15 (2010), https://doi.org/10.5004/dwt.2010.1756.
[15] P.A. Araújo, J.C. Kruithof, M.C.M. Van Loosdrecht, J.S. Vrouwenvelder, The potential of standard and modified feed spacers for biofouling control, J. Membr. Sci. 403–404 (2012), https://doi.org/10.1016/j.memsci.2012.02.015.
[16] A. Ronen, R. Semiat, C.G. Dosoretz, Impact of ZnO embedded feed spacer on biofilm development in membrane systems, Water Res. 47 (2013), https://doi.org/10.1016/j.watres.2013.08.036.
[17] C. Thamaraiselvan, Y. Carmiel, G. Eliad, C.N. Sukenik, R. Semiat, C.G. Dosoretz, Modification of a polypropylene feed spacer with metal oxide-thin film by chemical bath deposition for biofouling control in membrane filtration, J. Membr. Sci. 573 (2019) 511–519, https://doi.org/10.1016/J.MEMSCI.2018.12.033.
[18] H.L. Yang, J.C. Te Lin, C. Huang, Application of nanosilver surface modification to RO membrane and spacer for mitigating biofouling in seawater desalination, Water Res. 43 (2009), https://doi.org/10.1016/j.watres.2009.06.002.
[19] A. Ronen, S. Lerman, G.Z. Ramon, C.G. Dosoretz, Experimental characterization and numerical simulation of the anti-biofuling activity of nanosilver-modified feed spacers in membrane filtration, J. Membr. Sci. 475 (2015) 320–329, https://doi.org/10.1016/J.MEMSCI.2014.10.042.
[20] R. Hausman, I.C. Escobar, A comparison of silver- and copper-charged polypropylene feed spacers for biofouling control, J. Appl. Polym. Sci. 128 (2013), https://doi.org/10.1002/app.38164.
[21] D.J. Miller, P.A. Araújo, P.B. Correia, M.M. Ramsey, J.C. Kruithof, M.C.M. van Loosdrecht, B.D. Freeman, D.R. Paul, M. Whiteley, J.S. Vrouwenvelder, Short-term adhesion and long-term biofouling testing of polydopamine and poly(ethylene glycol) surface modifications of membranes and feed spacers for biofouling control, Water Res. 46 (2012) 3737–3753, https://doi.org/10.1016/J.WATRES.2012.03.058.
[22] C. Thamaraiselvan, E. Manderfeld, M.N. Kleinberg, A. Rosenhahn, C.J. Arnusch, Superhydrophobic candle soot as a low fouling stable coating on water treatment membrane feed spacers, ACS Appl. Bio Mater. 4 (2021), https://doi.org/10.1021/acsabm.0c01677.
[23] H. Kitano, K. Takeuchi, J. Ortiz-Medina, R. Cruz-Silva, A. Morelos-Gomez, M. Fujii, M. Obata, A. Yamanaka, S. Tejima, M. Fujishige, N. Akuzawa, A. Yamaguchi, M. Endo, Enhanced antifouling feed spacer made from a carbon nanotube-polypropylene nanocomposite, ACS Omega 4 (2019), https://doi.org/10.1021/acsomega.9b01757.
[24] L. Pisharody, C. Thamaraiselvan, E. Manderfeld, S.P. Singh, A. Rosenhahn, C. J. Arnusch, Antimicrobial and antibiofouling electrically conducting laser-induced graphene spacers in reverse osmosis membrane modules, Adv. Mater. Interfaces 9 (2022), https://doi.org/10.1002/admi.202201443.
[25] D. Rice, A.C. Barrios, Z. Xiao, A. Bogler, E. Bar-Zeev, F. Perreault, Development of anti-biofouling feed spacers to improve performance of reverse osmosis modules, Water Res. 145 (2018) 599–607, https://doi.org/10.1016/J.WATRES.2018.08.068.
[26] Y. Wibisono, K.E. El Obied, E.R. Cornelissen, A.J.B. Kemperman, K. Nijmeijer, Biofouling removal in spiral-wound nanofiltration elements using two-phase flow cleaning, J. Membr. Sci. 475 (2015), https://doi.org/10.1016/j.memsci.2014.10.016.
[27] K. Reid, M. Dixon, C. Pelekani, K. Jarvis, M. Willis, Y. Yu, Biofouling control by hydrophilic surface modification of polypropylene feed spacers by plasma polymerisation, Desalination 335 (2014), https://doi.org/10.1016/j.desal.2013.12.017.
[28] M. Tenjimbayashi, R. Togasawa, K. Manabe, T. Matsubayashi, T. Moriya, M. Komine, S. Shiratori, Liquid-infused smooth coating with transparency, super-durability, and extraordinary hydrophobicity, Adv. Funct. Mater. 26 (2016), https://doi.org/10.1002/adfm.201602546.
[29] C. Howell, A. Grinthal, S. Sunny, M. Aizenberg, J. Aizenberg, Designing liquid-infused surfaces for medical applications: a review, Adv. Mater. 30 (2018), https://doi.org/10.1002/adma.201802724.
[30] J.L. Yin, M.L. Mei, Q.L. Li, R. Xia, Z.H. Zhang, C.H. Chu, Self-cleaning and antibiofouling enamel surface by slippery liquid-infused technique, Sci. Rep. 6 (2016), https://doi.org/10.1038/srep25924.
[31] A.K. Epstein, T.S. Wong, R.A. Belisle, E.M. Boggs, J. Aizenberg, Liquid-infused structured surfaces with exceptional anti-biofouling performance, Proc. Natl. Acad. Sci. U. S. A. 109 (2012), https://doi.org/10.1073/pnas.1201973109.
[32] U. Manna, N. Raman, M.A. Welsh, Y.M. Zayas-Gonzalez, H.E. Blackwell, S. P. Palecek, D.M. Lynn, Slippery liquid-infused porous surfaces that prevent microbial surface fouling and kill non-adherent pathogens in surrounding media: a controlled release approach, Adv. Funct. Mater. 26 (2016), https://doi.org/10.1002/adfm.201505522.
[33] M.J. Kratochvil, M.A. Welsh, U. Manna, B.J. Ortiz, H.E. Blackwell, D.M. Lynn, Slippery liquid-infused porous surfaces that prevent bacterial surface fouling and inhibit virulence phenotypes in surrounding planktonic cells, ACS Infect. Dis. 2 (2016), https://doi.org/10.1021/acsinfec-dis.6b00065.
[34] Y. Kovalenko, I. Sotiri, J.V.I. Timonen, J.C. Overton, G. Holmes, J. Aizenberg, C. Howell, Bacterial interactions with immobilized liquid layers, Adv. Healthc. Mater. 6 (2017), https://doi.org/10.1002/adhm.201600948.
[35] C. Howell, T.L. Vu, J.J. Lin, S. Kolle, N. Juthani, E. Watson, J.C. Weaver, J. Alvarenga, J. Aizenberg, Self-replenishing vascularized fouling-release surfaces, ACS Appl. Mater. Interfaces 6 (2014), https://doi.org/10.1021/am503150y.
[36] T.S. Wong, S.H. Kang, S.K.Y. Tang, E.J. Smythe, B.D. Hatton, A. Grinthal, J. Aizenberg, Bio-inspired self-repairing slippery surfaces with pressure-stable omniphobicity, Nature 477 (2011), https://doi.org/10.1038/nature10447.
[37] C. Urata, G.J. Dunderdale, M.W. England, A. Hozumi, Self-lubricating organogels (SLUGs) with exceptional syneresis-induced anti-sticking properties against viscous emulsions and ices, J. Mater. Chem. A Mater. 3 (2015), https://doi.org/10.1039/c5ta02690c.
[38] N. Maccallum, C. Howell, P. Kim, D. Sun, R. Friedlander, J. Ranisau, O. Ahanotu, J. J. Lin, A. Vena, B. Hatton, T.S. Wong, J. Aizenberg, Liquid-infused silicone as a biofouling-free medical material, ACS Biomater Sci. Eng. 1 (2015) 43–51, https://doi.org/10.1021/ab5000578.
[39] K. Yu, Y. Han, A stable PEO-tethered PDMS surface having controllable wetting property by a swelling-deswelling process, Soft Matter 2 (2006), https://doi.org/10.1039/b602880m.
[40] U.W. Gedde, A. Hellebuych, M. Hedenqvist, Sorption of low molar mass silicones in silicone elastomers, Polym. Eng. Sci. 36 (1996) 2077–2082, https://doi.org/10.1002/pen.10603.
[41] R.J. Young, P.A. Lovell, Introduction to Polymers, Third edition, 2011, https://doi.org/10.1201/9781439894156.
[42] S. Kolle, O. Ahanotu, A. Meeks, S. Stafslien, M. Kreder, L. Vanderwal, L. Cohen, G. Waltz, C.S. Lim, D. Slocum, E.M. Greene, K. Hunsucker, G. Swain, D. Wendt, S.L. M. Teo, J. Aizenberg, On the mechanism of marine fouling-prevention performance of oil-containing silicone elastomers, Sci. Rep. 12 (2022), https://doi.org/10.1038/s41598-022-15553-4.
[43] F. Song, D. Ren, Stiffness of cross-linked poly(dimethylsiloxane) affects bacterial adhesion and antibiotic susceptibility of attached cells, Langmuir 30 (2014), https://doi.org/10.1021/la502029f.
[44] F. Li, F. Mugele, How to make sticky surfaces slippery: contact angle hysteresis in electro-wetting with alternating voltage, Appl. Phys. Lett. 92 (2008), https://doi.org/10.1063/1.2945803.
[45] I. Sotiri, A. Tajik, Y. Lai, C.T. Zhang, Y. Kovalenko, C.R. Nemr, H. Ledoux, J. Alvarenga, E. Johnson, H.S. Patanwala, J.V.I. Timonen, Y. Hu, J. Aizenberg, C. Howell, Tunability of liquid-infused silicone materials for biointerfaces, Biointerphases 13 (2018), https://doi.org/10.1116/1.5039514.
[46] DOW FILMTECTM™ Membranes, Cleaning Procedures for DOW FILMTEC FT30 Elements, Fact Sheet, 2009.
[47] Sterlitech corporation, RO/NF Cleaning Guidelines: Sterlitech Membranes Cleaning Procedures for, Product Information, 2015.
[48] J.N. Lee, C. Park, G.M. Whitesides, Solvent compatibility of poly (dimethylsiloxane)-based microfluidic devices, Anal. Chem. 75 (2003), https://doi.org/10.1021/ac0346712.
[49] G. Ducom, B. Laubie, A. Ohannessian, C. Chottier, P. Germain, V. Chatain, Hydrolysis of polydimethylsiloxane fluids in controlled aqueous solutions, Water Sci. Technol. 68 (2013), https://doi.org/10.2166/wst.2013.308.
[50] S.R. Khairkar, A.V. Pansare, A.A. Shedge, S.Y. Chhatre, A.K. Suresh, S. Chakrabarti, V.R. Patil, A.A. Nagarkar, Hydrophobic interpenetrating polyamide-PDMS membranes for desalination, pesticides removal and enhanced chlorine tolerance, Chemosphere 258 (2020), https://doi.org/10.1016/j.chemosphere.2020.127179.
[51] W. Lin, Y. Zhang, D. Li, X. Mao Wang, X. Huang, Roles and performance enhancement of feed spacer in spiral wound membrane modules for water treatment: a 20-year review on research evolvement, Water Res. 198 (2021), https://doi.org/10.1016/j.watres.2021.117146.